mAbs

ISSN: 1942-0862 (Print) 1942-0870 (Online) Journal homepage: https://www.tandfonline.com/loi/kmab20

The impact of proline isomerization on antigen binding and the analytical profile of a trispecific anti-HIV antibody

Masiero Alessandro, Lechat Nelly, Gentric Marianne, Sourrouille Christophe, Laville Florian, Crépin Ronan, Borel Claire, Ziegler Cornelia, Bisch Grégoire, Leclerc Eric, Laurent Ludovic, Brault Dominique, Alexandre Sylvie, Gagnaire Marie, Duffieux Francis, Soubrier Fabienne, Capdevila Cécile, Arnould Isabelle, Dumas Jacques, Dabin Jérôme, Genet Bruno, Radošević Katarina, Menet Jean-Michel & Prades Catherine

To cite this article: Masiero Alessandro, Lechat Nelly, Gentric Marianne, Sourrouille Christophe, Laville Florian, Crépin Ronan, Borel Claire, Ziegler Cornelia, Bisch Grégoire, Leclerc Eric, Laurent Ludovic, Brault Dominique, Alexandre Sylvie, Gagnaire Marie, Duffieux Francis, Soubrier Fabienne, Capdevila Cécile, Arnould Isabelle, Dumas Jacques, Dabin Jérôme, Genet Bruno, Radošević Katarina, Menet Jean-Michel & Prades Catherine (2019): The impact of proline isomerization on antigen binding and the analytical profile of a trispecific anti-HIV antibody, mAbs, DOI: 10.1080/19420862.2019.1698128

To link to this article: https://doi.org/10.1080/19420862.2019.1698128

Publisher: Taylor & Francis

Journal: *mAbs*

DOI: 10.1080/19420862.2019.1698128

The impact of proline isomerization on antigen binding and the analytical profile of a trispecific anti-HIV antibody

Masiero Alessandro[1‡], Lechat Nelly[2‡], Gentric Marianne[2], Sourrouille Christophe[2], Laville Florian[2], Crépin Ronan[2], Borel Claire[2], Ziegler Cornelia[2], Bisch Grégoire[2], Leclerc Eric[2], Laurent Ludovic[2], Brault Dominique[2], Alexandre Sylvie[2], Gagnaire Marie[1], Duffieux Francis[1], Soubrier Fabienne[1], Capdevila Cécile[1], Arnould Isabelle[1], Dumas Jacques[1], Dabin Jérôme[2], Genet Bruno[2], Radošević Katarina[1], Menet Jean-Michel[2], Prades Catherine[1*]

[1]Biologics Research and [2]Biologics Development, SANOFI R&D, 94400 Vitry-sur-Seine, France

‡These authors contributed equally

**Corresponding author: Catherine Prades, catherine.prades@sanofi.com*

Abstract

Proline *cis-trans* conformational isomerization is a mechanism that affects different types of protein functions and behaviors. Using analytical characterization, structural analysis and molecular dynamics simulations, we studied the causes of an aberrant two-peak size exclusion chromatography profile observed for a trispecific anti-HIV antibody. We found that proline isomerization in the tyrosine-proline-proline (YPP) motif in the heavy chain complementarity-determining region (CDR)3 domain of one of the antibody arms (10e8v4) was a component of this profile. The pH effect on the conformational equilibrium that led to these two populations was presumably caused by a histidine residue (H147) in the light chain that is in direct contact with the YPP motif. Finally, we demonstrated that, due to chemical equilibrium between the *cis* and *trans* proline conformers, the antigen binding potency of the trispecific anti-HIV antibody was not significantly affected in spite of a potential structural clash of 10e8v4 $YP_{trans}P_{\mathbf{trans}}$ conformers with the membrane proximal ectodomain region epitope in the GP41 antigen. Altogether, these results reveal at mechanistic and molecular levels the effect of proline isomerization in the CDR on the antibody binding and analytical profiles, and support further development of the trispecific anti-HIV antibody.

Keywords: proline isomerization, antibody conformers, chemical equilibrium, developability

Introduction

Biopharmaceutical development of antibodies requires solid understanding of antibody structure and function in order to design appropriate manufacturing and analytical methodologies. This aspect becomes even more important with the rise of more complex antibody formats, such as multispecific antibodies,[1–3] that also pose substantial challenges in terms of antibody engineering. In-depth understanding of antibody chemistry can yield valuable information for the rational design of improved antibody variants, as well as for the assessment of the potential development risks. During pre-clinical development of our unique and therapeutically promising trispecific antibody against HIV,[4] we observed an aberrant native size-exclusion chromatography-mass spectrometry (SEC-MS) profile, which suggested a conformational isomerization.

Peptide bonds in proteins, including antibodies, are often planar due to their partially double bond nature, and the relative isomeric conformation of Cα atoms with respect to the C-N peptide bond is typically *trans*, yielding dihedral values close to 180°. The *cis* conformation, with dihedral angle close to 0°, is usually energetically unfavorable and thus less probable.[5] In general, *trans-cis* conformers have an energetic difference of approximately 2-6 kcal/mol,[6] while the *trans-cis* conformational switching activation energy to overcome is ~20 kcal/mol.[6,7] For proline, due to its particular closed five-atom ring sidechain, the energetic cost of *trans-cis* conformational switching is lower (~2 kcal/mol less),[8] with interconversion kinetics ranging from seconds to minutes.[7] This proline isomerization is in chemical equilibrium, thus the same molecular entity can form *cis* and *trans* conformers simultaneously, as observed in protein crystal structures.[5] Different variables, such as temperature or pH, can shift the equilibrium from one population to another or enrich either conformation state.[9] Another important factor that affects the *cis/trans* ratio is the type of amino acid preceding proline. Prolines preceded by aromatic residues such as tyrosine or phenylalanine, or another proline, are more likely to adopt cis conformation.[5,10] Proline isomerization forms the basis of some molecular allosteric switches[10,11] and timers,[13] and plays a role in different physiological (e.g., immune function,[14] cell signaling[15–18]) and pathological conditions (e.g., cancer,[19–22] Alzheimer's disease[19,23]). In a classical antibody structure, prolines can be found both in constant and variable regions. In constant regions, they participate in domain folding (i.e., CH2,[24] CH3,[25] scFv[25] folding pathways) after quaternary structure formation, by the enzymatic activity of prolyl isomerases.[27] The prolyl isomerization in antibody complementarity-determining regions (CDRs) can occur upon

antigen binding,[7] but in general it is a rare event.

Our trispecific anti-HIV antibody (SAR441236) consists of variable domains of three different monoclonal antibodies (mAbs) (VRC01,[28,29] PGDM1400[30] and 10e8v4[29,31]) arranged in a novel IgG1 scaffold, with one classical antigen-binding fragment (Fab) arm (VRC01 Fab) and a CODV[32] bispecific dual variable domain arm (PGDM1400 and 10e8v4).[4] In order to understand the unusual two-peak SEC profile of this antibody, we characterized the nature of the two peaks using experimental and computational methods. Our results revealed a key role for prolines at position 112 and 113 (belonging to the YPP motif) of the heavy chain CDR3, and histidine at position 147 of the light chain of the antibody 10e8v4.

Results

Analytical characterization

Ultra-high performance liquid chromatography-SEC (UHPLC-SEC) analysis of the trispecific anti-HIV antibody demonstrated an unusual elution profile, with two non-resolved peaks, indicating sample heterogeneity (Figure 1A). This heterogeneity could not be confirmed using dynamic light scattering (DLS), SEC-MALS or sedimentation velocity analytical ultra-centrifugation (SV-AUC) (*data not shown*). The peaks were separated using SEC – light scattering (SEC-LS) analysis, yielding two peaks with the same apparent molecular weight (~ 200 kDa) and hydrodynamic radius (6.4 nm) (Figure 1B), which suggested the presence of different conformers. Using SEC-MS in denaturing conditions on deglycosylated material, the trispecific antibody eluted in one peak and the deconvoluted spectra of this peak demonstrated a single molecular weight entity, further supporting the conformer hypothesis (Figure 1C). The antibody was also analyzed using SEC-native MS and the deconvolution of the combined spectra of each peak confirmed the presence of two species with the same molecular weight (Suppl. Figure 1). The stability of conformers was probed according to the protocol described by Kwon et al.[31] The two peaks observed on the SEC profile were fractionated and fractions were analyzed using SEC either immediately after collection or after storage at 8°C for 72h (Figure 1D). Immediately after separation, the individual fractions were dominated by the isolated conformer, but after 72h the conformers reached the same equilibrium in both fractions, with a conformational equilibrium of approximately 60:40, suggesting conformational isomerization as a likely mechanism (Figure 1D and 1E). To determine the effect of pH on the reversibility of these two conformer populations, we analyzed the samples for conformer peak ratio after changing sample buffer pH from pH 6.0 to pH 5.0, and then to pH 7 (Figure 1E). The equilibrium ratio between two conformers depended on pH and was completely reversible, suggesting the presence of a pH-sensing residue in the vicinity of conformational switching site.

In order to elucidate which component of the trispecific anti-HIV antibody was responsible for the appearance of the two conformers, the trispecific antibody was digested by a FabALACTICA® protease that cleaves above the hinge region, leading to three fragments: 1) a Fc (~ 53 kDa); 2) CODV PGDM1400-10e8v4 (~79 kDa); and 3) Fab VRC01 (~ 50 kDa) (Figure 2A). The digestion mix was separated and analyzed using SEC/UV-MS, exhibiting

three major peaks between 9 and 12 min, with two minor peaks originating from the protease appearing between 7 and 9 min (Figure 2B). The peak eluting at 9.6 min was confirmed by MS to be a mixture of the Fc and the VRC01 Fab. The two peaks with the same molecular weight and eluting at 9.2 and 11.7 min, respectively, both corresponded to PGDM1400-10e8v4 CODV arm. This result demonstrates that CODV PGDM1400-10e8v4 was responsible for the generation of two conformers and the atypical behavior on the SEC column. Previous work had shown that the parental 10e8v4, one of the two antibodies in the CODV arm, also exhibited an anomaly in SEC as a mAb, likely related to slow conformational isomerization of heavy chain CDR3.[31] Therefore, we focused on further characterization of the 10e8v4 in CODV arm.

Structural characterization

In order to elucidate the molecular basis for the occurrence of 10e8v4 conformers in the trispecific anti-HIV antibody, we analyzed the crystal structures of the 10e8v4 mAb Fab in complex with its antigen GP41, and of the CODV PGDM1400-10e8v4 bispecific arm from the trispecific antibody (Protein Data Bank IDs: 5IQ9[31] and 5WHZ,[4] respectively). Superimposing the two structures revealed excellent resemblance, but also a clear difference between the heavy chain CDR3 loops of 10e8v4 in both structures, with a more "closed" structure in monospecific 10e8v4 Fab and a more "open" structure in 10e8v4 in bispecific CODV (Figure 3A). The difference between the two structures was primarily due to proline 113 in the Y111-P112-P113 motif of the heavy chain CDR3, which adopted a *cis* conformation in the monospecific Fab and a *trans* conformation in the bispecific CODV arm, with proline 112 adopting the *trans* conformation in both structures (Figure 3B). Importantly, the crystal structures had been generated at different pH: the 10e8v4-GP41 co-crystal was generated at pH 8.5, whereas the CODV crystal was obtained at pH 6.1. Since a more "open" conformation of CDR would lead to more exposure of hydrophobic patches, we probed the difference in hydrophobicity as a proxy for conformation, using 1-anilinonaphthalene-8-sulfonate (ANS) fluorescent dye exhibiting a blue shift upon exposure to a more hydrophobic environment.[33] A significant blue shift was observed at pH 5 but not at pH 7, confirming that at low pH the trispecific anti-HIV antibody molecules indeed adopts a more "open" conformation (Suppl. Table 1). The fact that we observed two conformations in crystals obtained at different pH confirms the results presented in Fig. 1D, and demonstrates that pH has a profound impact on the conformation of 10e8v4 heavy chain CDR3. The observed pH

dependence of the conformational switch site can probably be explained by the close proximity of histidine 147 of the 10e8v4 light chain, which is in direct contact with heavy chain CDR3 through a hydrogen bond with glycine 114 (Figure 3C). We hypothesize that the pH change from basic to acidic changes H147 protonation state from single to double protonated, which causes steric hindrance due to supplementary hydrogen atom and charge repulsion with arginine 207. The charge repulsion, in turn, could yield the disruption of the hydrogen bond between H147 of the light chain and G114 of the heavy chain, which results in the "open" conformation.

Antigen binding characterization

During structural analysis, we observed that the 10e8v4 P113 in *trans* conformation may cause steric clash with its cognate epitope membrane proximal ectodomain region (MPER) (Suppl. Figure 2), and thus affect antibody-antigen binding. To verify the impact of this conformational change on antibody binding, the two conformers of trispecific anti-HIV antibodies were purified and their binding to GP41 MPER antigen was evaluated.

The ELISA dose-response binding curves demonstrate that purified P113 *cis* conformer exhibits a significantly lower EC_{50} compared to the *trans* conformer and a comparable EC_{50} to a reference batch (batch with both conformers in equilibrium) (Figure 4). Additionally, the sensorgrams and kinetic parameters determined using biolayer interferometry (BLI) show a 10-fold difference in the K_D values between the two conformers (Table 1 and Suppl. Fig. 3), with *cis* conformer having higher affinity, and the observed difference being mainly due to the difference is association rates (ka). In agreement with ELISA data, the mixture of conformers shows a kinetic profile close to the more potent *cis* conformer.

In addition, we analyzed the kinetics of the trispecific anti-HIV antibody/GP41 antigen complex formation using SEC and UV_{280} (Figure 5, Suppl. Fig 4). In agreement with the BLI results, we observed instantaneous binding to GP41 for the *cis* conformer and much slower binding for the *trans* conformer, with the increase of antibody-antigen complex accordingly compensated by the decrease of the two uncomplexed conformers. In SEC-MS, both anti-HIV antibody conformers exhibited the same association with the epitopes of the two other antibodies forming the trispecific anti-HIV antibody (VRC01 and PGDM1400) (*data not shown*), indicating that the observed conformational change only affects 10e8v4 binding.

Together, these results demonstrate that the two conformers of trispecific anti-HIV antibody exhibit different GP41 binding characteristics due to a conformational change in the YPP motif within 10e8v4 HCDR3.

Molecular Dynamics Simulations

The P113 is a part of tyrosine-proline-proline (Y111-P112-P113) motif and we used molecular dynamics simulations to determine which *cis*-*trans* conformation transitions of the two prolines would be energetically the most favored. The 10e8v4 Fab was analyzed by means of four enhanced sampling accelerated[34] molecular dynamics simulations. Root mean square deviation (RMSD) and root mean square fluctuation (RMSF) plots were generated on fitted trajectories to verify the correct folding of the proteins over 4x100 ns, and in all systems the main observed population was at 5Å or below, indicating no major unfolding events (Suppl. Figure 5).

The dihedral angles between the Cα atoms with respect to C-N backbone of the two neighboring residues of the YPP motif (e.g., Y111-P112, P112-P113) were measured to determine whether they are preferentially adopting *cis* (dihedral angle close to 0°) or *trans* (dihedral angle close to 180°) conformation (Figure 6). The simulations revealed that the P112-P113 could potentially adopt all four possible conformations *(trans*-*trans, trans*-*cis, cis*-*cis, cis*-*trans*), but with the clear differences in the population densities and transition probabilities (Figure 6). The *trans*P112-*trans*P113 state was the most populated, thus the most preferred conformation, suggesting the highest energetic stability of *trans* Cα atoms for adjacent residues. The *cis*P112-*cis*P113 conformation appeared to be the least favorable both in terms of conformational population and transition states leading to it. Another populated conformation is *cis*P112-*trans*P113, but the pathways between this conformation and the other ones were not populated, suggesting a higher transition energetic barrier between this conformation and the other conformations, and thus less likelihood of this transition. Both *trans*P112-*cis*P113 and *trans*P112-*trans*P113 states were well populated, suggesting that these two conformations are more likely than other conformations. More population density between *trans*P112-*trans*P113 and *trans*P112-*cis*P113 than between *trans*P112-*trans*P113 and *cis*P112-*trans*P113 suggests that the energetic barrier for *trans*P112-*trans*P113 to switch to *trans*P112-*cis*P113 is lower, and thus more likely than conversion to *cis*P112-*trans*P113. Moreover, compared to the *cis*P112 peak, the *cis*P113 peak is skewed towards the *trans* state.

This suggests that the structure surrounding this proline biases its conformation towards a *cis* to *trans* transition (Figure 6). This is also corroborated by the count of frames showing dihedral angle values between 45° and 135°, with ~12500 over 100000 for P113 and ~2300 over 100000 for P112.

Our modeling results can be translated to the following equilibrium:

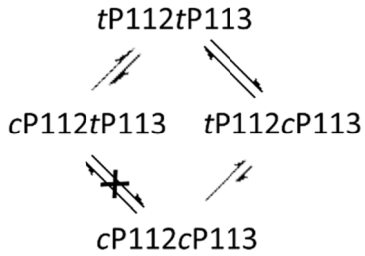

These results suggest that P113 is the most involved residue in *cis-trans* conformational switching, and thus likely the main contributor to conformational transitions.

In order to verify the conformational equilibrium hypothesis and the effects of the YPP motif on antibody binding and the SEC profile, we generated the following antibody mutants: P113A (var1), P112A (var2), P112A/P113A (Var3) and Y111A/P112A (Var4). Since we hypothesized that the observed effect of pH on antibody binding and isomerization state was due to H147, which is in direct contact with HCDR3, we also generated mutant H147A (Var5). Following the production of these variants, we evaluated the effect of each mutation on the SEC profile (as a proxy for conformation) and antigen binding (Figure 7). For all mutant variants, we observed only one peak in native SEC, with the retention time in the range of retention times for the wild type conformers (Figure 7A). These chromatograms confirm that both the YPP motif in CDR3 of HC 10E8V4 and the H147 in CDR1 of light chain (LC) 10E8V4 have a direct impact on trispecific antibody *cis-trans* conformational switching.

The binding of each mutant variant to GP41 antigen was significantly lower compared to the wild type molecules (Figure 7B). Mutating P113 led to the most pronounced loss of binding, followed by H147 mutation and to a lesser extend P112, ranking the importance of these residues for antigen binding. This effect on binding may be due either to the impact on conformational changes elicited by these mutations or direct involvement of these residues in antigen binding. Based on the crystal structure, we know that neither HCDR3 P113 nor light

chain H147 side chains directly interact with the antigen, and the P112 side chain only exhibits minor contacts. Despite this, the mutation of these residues to alanine significantly affected antigen binding, corroborating the conformational switching as the major cause.

Based on our results, we conclude that both the YPP motif and histidine are essential for the optimal binding to MPER antigen and must be kept intact in the antibody to preserve its potency.

Discussion

The impact of proline isomerization on the biological functions of proteins has been widely documented.[12,13,20,21,35,36] Proline isomerization has also been documented as a driver for proper folding of antibody constant domains, facilitated by prolyl isomerases.[24–27,37,38] Despite the bimodal behavior of proline, only one conformation is generally compatible with the native structure of antibodies.[38] An exception has been reported by Shinoda *et al.,* who have shown that antigen binding can lead to proline isomerization and generation of both conformers in a CDR.[7]

In this work, we characterized the impact of proline isomerization in the CDR on the functional and analytical profile of a trispecific anti-HIV antibody.[4] This antibody, consisting of three different HIV-specific binding arms in one molecule (VRC01 as a Fab and PGDM1400-10e8v4 in CODV[32] arm), has shown promising results in preclinical HIV models and is currently being tested in a Phase 1 clinical study (NCT03705169).[4] We demonstrate that proline isomerization in the HCDR3 Y111-P112-P113 motif, assisted with pH-sensing by H147 in the LC of the 10e8v4 antibody arm, is the key phenomenon driving the aberrant behavior of the antibody observed in SEC. This behavior was not due to the trispecific format of the molecule, since an anomaly in the SEC profile was also previously detected with the 10e8v4 mAb.[31,39] We identified proline 113 isomerization as a possible cause of the two-peak SEC profile based on subtle differences between antibody-antigen complex crystal structures obtained at different pH. At less acidic conditions, HCDR exhibited more “closed” structure and P113 adopted *cis* conformation, while at pH 6.1 a more “open” CDR structure and P113 *trans* isomers were observed. The “closed” *cis* conformer bound GP41 antigen with higher affinity than the “open” *trans* conformer, reflecting the structural clash between epitope and *trans* conformer as anticipated from the crystal structure. The samples with purified *cis* isomers demonstrated only a slight difference in antigen binding versus sample containing

mixed isomers. As we have shown that the equilibrium between the two conformers is re-established immediately after purification of either conformer, the lack of significant difference in binding between the *cis* conformer and the mixed sample may be explained by fast sequestration of the more affine *cis* conformer by the antigen, and consequent re-equilibration of the conformers. This is a very important finding from the perspective of developing the trispecific anti-HIV antibody as a biotherapeutic, since it indicates that the presence of two isomers does not significantly affect the potency of the molecule, and thus does not require additional engineering. Engineering to fix the aberrant SEC profile in this antibody should in fact be avoided because Kwon *et al*[31] reported that, although the observed SEC anomaly of 10e8v4 mAb could be restored to a classical single peak by engineering a disulfide bond between Y100C (corresponding to Y111 for the trispecific) in HCDR3 and S30C (corresponding to S140 for the trispecific) in LCDR1, this came at the expense of significant loss of antibody potency.

We also demonstrated that proline/alanine mutations designed to raise the energetic barrier between *cis* and *trans* conformation transitions[6] restored the single peak in SEC, but this also led to significant loss of antibody binding. However, the phenomenon appears to be more complex than a simple YPP isomerization event. The mutation of presumed pH-sensing H147 in LC also yields a single SEC peak, despite maintaining the YPP motif in the HCDR3 loop. The bulky H147 may constitute a steric hindrance for the complete positioning of HCDR3 over the light chain variable domain, and in this way sterically impact the YPP isomerization. Moreover, histidine is known to have three different protonation states. The conversion between single protonated neutral histidine and double protonated positively charged histidine occurs at pH <6, and we demonstrated that changing pH from neutral to pH 5 led to a (reversible) change in the ratio between *cis*P113 and *trans*P113 conformers. The reversibility of the conformational population following pH change ensures that at a given pH the behavior will remain unchanged. The combined effect of the YPP motif in the heavy chain and H147 in the light chain demonstrates that both these elements are important in the formation of the two conformers. Although we cannot exclude that the mutation of these residues could directly impact antigen contact, the crystal structures demonstrate no major interaction between the side chains and the antigen, thus indicating that the conformational switching is the basis of antigen binding disruption.

The molecular dynamics simulations suggest that *trans*P112-*trans*P113 and *trans*P112-*cis*P113 are the most likely occurring conformations. Other conformations, such as

*cis*P112-*cis*P113 and *cis*P112-*trans*P113, are theoretically possible, but the preferred transition state as observed by enhanced conformational sampling reinforces the bimodal conformational equilibrium between *trans*P112-*trans*P113 and *trans*P112-*cis*P113. Nevertheless, we cannot exclude the concomitant existence of all four conformers, as the differences between the four states could be too small to be detected by SEC.

The five mutation variants confirm that each residue highlighted in this study (i.e., YPP and H147) plays a role in the isomerization phenomenon, with P113 being the most important residue and the actual switching site. This is in concordance with previously published work that indicated that the presence of either an aromatic residue (especially tyrosine, tryptophan and phenylalanine) or a proline residue itself preceding a proline in a Xaa-P dipeptide[5,10] must be carefully taken into account during protein engineering. If the aromatic-proline-proline motif is close to a flexible loop with a few conformational constraints to lock it in place, a conformational equilibrium is potentially enabled. Indeed, another relevant parameter that might be co-responsible for this phenomenon in our study is the relatively long HCDR3 loop of 10e8v4 antibody (22 residues). We cannot exclude the possibility that a shorter CDR3 loop containing the same motif would show typical profiles in SEC. However, shortening the CDR loop for this particular antibody is not an option since it would very likely negatively impact antigen binding. Further investigations, beyond the scope of our study, are needed to elucidate the effect of antibody CDR loop length and composition, together with proline isomerization sites, on small-middle range conformational movements and their analytical consequences.

Together, our results demonstrate that the presence of proline and histidine and the related conformational switching in CDRs are highly relevant for antibody functional and analytical behavior. Moreover, our description of an additional antibody with proline isomerization in the CDR region suggests that CDR proline isomerization might be a phenomenon more common than previously thought. Understanding these features is highly informative for designing appropriate strategies for biotherapeutics development.

Materials and methods

Protein Production, Purification and Characterization

The trispecific CODV-Ig protein SAR441236 is composed of a CODV arm containing two variable regions (10e8V4 and PGDM1400) and of a Fab arm containing the variable region VRC01.[23] Therefore, six plasmids were designed: five encoding the CODV arm with either one or two mutations: P112A, P113A, P112A-P113A, Y111A-P112A in the HC or H147A in the LC, one encoding the Fab arm that was common to the five mutants. Plasmid encoding the Fab arm contained selection marker 1, while plasmids encoding mutated CODV arm contained selection marker 2. Coding sequences were obtained by gene synthesis and codon usage was optimized for *Cricetulus griseus* (GeneArt). Sanofi's proprietary Chinese hamster ovary (CHO) cell line was first electroporated with the plasmid encoding the Fab arm and cells were grown in CD OptiCHO medium (Gibco) with selection maker 1. Once cells recovered a cell viability of 90%, the second electrotransfection was performed with one of the plasmids encoding the mutated CODV arm. Cells were grown several days in CD OptiCHO medium with both selection markers 1 and 2. Once cells recovered a cell viability of 90%, scale up was performed to a volume of 1.5 L. At a cell viability of 70% (12-14 days), cells were removed by centrifugation and cell supernatants were filtered on 0.22 µm membrane. Cell supernatants were stored at 2-8 °C until purification. Clarified supernatants were applied on Protein A columns equilibrated with Dulbecco phosphate-buffered saline (DPBS) buffer (Gibco). Trispecific CODV-Ig protein mutants were eluted with an acidic pH buffer (2.8), neutralized, filtered on a 0.22 µm membrane and applied on HiLoad 26/600 Superdex 200 PG columns (GE Healthcare) in order to remove high molecular weight products. Fractions corresponding to the monomeric form of each CODV-Ig protein mutant were pooled, concentrated using Centriprep Centrifugal Filter Unit (10 kDa cutoff, EMD) to 10 mg/mL. The protein batches were stored at 2-8 °C and analyzed by capillary electrophoresis (in reducing and non-reducing conditions), analytical SEC and MS (in reducing condition).

Conformer collection: Purifications are carried out using a SEC column (Waters XBridge BEH200 (7.8*300mm). An isocratic elution using DPBS2X, pH 7.0 at 1 mL/min was used for chromatographic separation Ultimate 3000 LC-UV system (ThermoFisher Scientific) comprising a quaternary pump, a sample manager set at 5 °C, a column oven set at 15 °C and a UV detector operating at 254 nM. Fractions were collected at 7.1 min and 9.1 min during 40 sec.

Size-exclusion chromatography

Size-exclusion chromatography with light scattering: The separation of SAR441236 solution was performed by SEC using an Agilent HPLC system and a ProSEC 300 x 7.5 mm column (Agilent Technologies) controlled at 25 °C. The eluent, DPBS 4X (dilution of DPBS 10X, BE17-515F Lonza)) was pumped at 0.3 ml/min. Detection was carried out using Agilent UV (280 nm), miniDAWN light scattering (Wyatt Technology) and Dynapro dynamic light scattering (Wyatt technology) detectors. Determination of molecular weight and hydrodynamic radius was performed by the astra VI software (Wyatt Technology). The refractive index increment (dn/dc) value of 0.185 ml/g and a UV extinction coefficient (dA/dC) of 1.667 ml/(mg.cm) was used for the molecular weight determination.

Size-exclusion chromatography - Mass Spectrometry in denaturing condition: Antibody samples were diluted to 1 mg/mL using MilliQ Water. 1 µg was injected on an Acquity UHPLC IClass (Waters, Manchester, UK) comprising a binary pump, a sample manager set at 10 °C, a column oven and a TUV detector operating at 280 nm. The desalting was performed with a Waters SEC column (BEH200A 1.7 µm, 300 mm X 4.6 mm) in isocratic elution with a mobile phase of ammonium formate 25 mM with 1% formic acid / acetonitrile (70/30), and the flow rate set at 0.3 ml/min. The UHPLC was coupled to a mass spectrometer QToF G2Si (Waters, Manchester, UK) and the analysis was performed via electrospray ionization (ESI) in positive mode.

Size-exclusion chromatography in native conditions directly coupled to ESI-MS: The native SEC-UV/MS was carried out using a SEC column (BEH SEC 200A, 4.6 × 300 mm, 1.7 µm particle size; Waters, Milford, MA, USA). An isocratic elution using 100 mM CH_3COONH_4, pH 6.8 at 0.3 mL/min was used for chromatographic separation on a SCIEX EXION LC (Framingham, MA, USA), comprising a binary pump, a sample manager set at 10 °C, a column oven and a UV detector operating at 280 nM. The UHPLC system was coupled to a SCIEX X500B mass spectrometer (Framingham, MA, USA). Antibody samples were diluted to 15 mg/mL using MilliQ Water. Sample injection amounts of 75 µg were used and data acquisition was controlled by SCIEX OS (Framingham, MA, USA). The X500B was operated in positive mode (ESI).

Sample preparation for subunits digestion: IgdE (FabALACTICA®) immunoglobulin-degrading protease was obtained from Genovis AB (Lund, Sweden). For enzymatic digestion,

200 units of FabALACTICA® protease (Genovis) were added to 200 µg of mAb. The mix was digested overnight at 37 °C and 10 µl were loaded onto the SEC column operated in native condition.

Sample preparation for association kinetic with antigen and UHPLC analytical conditions: For the kinetic of association, 8.8 nMoles of GP41 MPER antigen and 4.4 nMoles of mAb were mixed in a vial. An aliquot of the reaction (5 µl) at T0, 5, 20, 40, 75 and 110 min was injected on an Acquity UHPLC Waters operated in native conditions as described above, with UV detection only.

Antigen Binding Characterization

ELISA: The GP41 MPER antigen was coated on 96-well plate overnight at +2/+8°C the day before. After a blocking step, with Tris-Buffered Saline (TBS)-bovine serum albumin 1% two preparations of the SAR441236 antibody concentrations from approximately 125 µg/mL to 0.002 µg/mL were applied in triplicate and incubated 1 hour at 22 °C on every plate. After a wash step with TBS-Tween 0.1%, a goat anti-human IgG (H+L) conjugated to horseradish peroxidase was added into the plates and incubated 1 hour at 22 °C. After a wash step with TBS-Tween 0.1%, the 3,3',5,5'-tétraméthylbenzidine substrate was finally added into the plates and incubated for 7 min. The peroxidase catalyzes a chemical reaction resulting in a colorimetric change. This colorimetric reaction was stopped using the STOP solution and the optical densities (OD) were measured at a wavelength of 450 nm using a spectrophotometer. The dose-response curves were generated with an internal application (Biost@t-Bioassay), using a 4-parameter model (OD versus antibody concentration in µg/mL). The effective concentration for which 50% of the maximum response is measured (EC_{50} in µg/mL) was determined by the application.

Octet binding: The biotinylated MPER peptide (MPERbiot) was captured on a Streptavidin sensor. The conformer fraction (fraction #1 or fraction #2) was used as analyte. Assays were run on a ForteBio Octet machine (BLI technology). MPERbiot (Innovative Peptide Solutions, ref #31571_1a) was captured on a streptavidin sensor (ref#18-0009), at a concentration of 0.8 µg/mL. The running buffer was 2X DPBS Tween 20 0.05%. To avoid bulk effects, all the dilutions were done in the running buffer. The conformer fraction collected from SEC purification was adjusted at a concentration of 600 nM, first point of a two-fold serial dilution (600 nM to 9.35 nM). The biotinylated MPER peptide has been loaded for 100 seconds.

Conformer association and dissociation phases were monitored for 300s and 600s, respectively, at 1000 RPM. Association step was achieved within 20 min after SEC purification to avoid return to the equilibrium state between conformers. Sensorgrams are subtracted with a buffer sensorgram and are fitted with a 1:1 model.

pH dependent kinetics

The SEC-UV was carried out using a SEC column (BEH SEC 200A, 4.6 × 300 mm, 1.7 µm particle size; Waters). An isocratic elution using DPBS 4X, pH 7.0 at 0.3 mL/min was used for chromatographic separation with an Acquity UHPLC HClass (Waters), comprising a quaternary pump, a sample manager set at 25 °C, a column oven set at 25 °C and a UV detector operating at 280 nm. Data acquisition and data processing were performed with Empower 3 Software. Antibody sample at 25 mg/mL was formulated in histidine pH 6.0. Five hundred µL of sample were loaded in Amicon Ultra 0.5 mL 10K filter (Millipore), centrifuged 15 min at 14000 g, and then rinsed three times with ammonium acetate pH 5.0. Remaining solution was titered and diluted to 5 mg/mL in ammonium acetate. Sample injection amounts of 20 µg were analyzed at t 0, 15 min, 30 min, 45 min, 1h, 1h 15 min, 1h 30 min, 1h 45 min and 2 h. Five hundred µL of sample at pH 5.0 at 5 mg/mL were loaded in Amicon Ultra 0.5 mL 10K filter (Millipore) centrifuged 15 min at 14000g and then rinsed three times with DPBS 4X pH 7.0 (Gilco). Remaining solution were tittered and diluted to 1 mg/mL in DPBS. Sample injection amounts of 4 µg were analyzed at T0, 15 min, 30 min, 45 min, 1 h, 1h 15 min, 1h 30 min, 1h 45 min, 2 h, 3 h, 4 h and 5 h.

Structural Analysis

Structural comparison has been performed by means of BIOVIA Discovery Studio suite 2018. The variable domains of the parental 10e8v4 Fab (PDB ID: 5IQ9,[31] resolution 2.4Å) and the CODV formatted 10e8v4 structure (PDB ID: 5WHZ,[4] resolution 3.549Å) were superposed by Cα structural alignment, obtaining a RMSD value of 1.056 Å. Aggregation surfaces were calculated by SAP[40] on both variable parts.

Molecular Dynamics Simulations

All molecular dynamics simulations were carried out by means of NAMD (v. 2.13)[41] with CHARMM27[42] force-field on the monospecific parental Fab (PDB ID: 5IQ9[31]). The system was placed in an orthorhombic TIP3p water box, the boundaries of which were placed at least

9Å far from the furthest protein atom, generating an ~80x72x80Å^3 solvent box for a total number of atoms of ~50000. The charge neutrality of the system and a physiological concentration of 0.15 M were used to place 38 Na^+ and 45 Cl^- ions. The simulation temperature was kept at 300 K and the pressure was kept at 1 atm in constant number of particles, pressure and temperature (NPT) ensemble. Protein protonation state assignment and system parameterization at pH 7 were performed by means of BIOVIA Discovery Studio 2018 suite. Accelerated molecular dynamics protocol[34] was applied, with dihedral boost potential, to enhance conformational sampling. The system underwent energy minimization, 100 ps in NVT (constant number of particles, volume and temperature) ensemble, 100 ps in NPT ensemble and an additional 1 ns of NPT molecular dynamics simulation to derive energy boost parameters for accelerated molecular dynamics. Four simulations of 100 ns each were run in a GPU Linux cluster, all in the NPT ensemble. RMSD and RMSF analyses were carried out after trajectory fitting and solvent removal, performed by Carma,[43] for the four systems, and dihedral for P112 and P113 were plotted over time to estimate *cis-trans* conformational switching over time by means of Bio3D[44] R package and VMD.[45] The conformational population was plotted by assigning each proline dihedral to a Cartesian graphic axe (x for P112 and y for P113).

Fluorescence Assay

The fluorescence assay was performed on a Xenius XL (SAFAS, Monaco), with an excitation wavelength 350 nm and an emission spectrum measured between 400 – 550 nm at 22 °C. Formulated protein samples were diluted either in PBS at pH 5 or pH 7 to 15 g/l final concentration and the samples were measured directly (t_0) and after 3 h of incubation time at room temperature. In both cases, 40 µM ANS final concentration was added prior to measurement. The fluorescence emission spectra were smoothed before the determination of the wavelength at maximum fluorescence intensity. Data were acquired in triplicates at three different days. Statistical analyses (unpaired t-test) were performed with GraphPad Prism 8.0 (GraphPad Software Inc., CA).

Acknowledgements

The authors are very thankful to Wouter Koudstaal (Lucidity Biomedical Consulting) and Isabel Lefevre for the editorial support, Thomas Bouquin, Marie-Thérèse David-Comte and Marc Ferron for their support, and to Laurence Parisot and the e-Biology team, Biologics Research France and Biologics Development France for all the insightful and fruitful discussions.

This work was funded by Sanofi R&D. No potential conflict of interest was reported by the authors.

Bibliography

1. Chen, S. *et al.* Immunoglobulin Gamma-Like Therapeutic Bispecific Antibody Formats for Tumor Therapy. *J. Immunol. Res.* **2019**, (2019).

2. Brinkmann, U. & Kontermann, R. E. The making of bispecific antibodies. *mAbs* **9**, 182–212 (2017).

3. Hu, W., Wang, G., Huang, D., Sui, M. & Xu, Y. Cancer Immunotherapy Based on Natural Killer Cells: Current Progress and New Opportunities. *Front. Immunol.* **10**, (2019).

4. Xu, L. *et al.* Trispecific broadly neutralizing HIV antibodies mediate potent SHIV protection in macaques. *Science* **358**, 85–90 (2017).

5. Reimer, U. *et al.* Side-chain effects on peptidyl-prolyl cis/trans isomerisation. *J. Mol. Biol.* **279**, 449–460 (1998).

6. Alderson, T. R., Lee, J. H., Charlier, C., Ying, J. & Bax, A. Propensity for cis-Proline Formation in Unfolded Proteins. *ChemBioChem* **19**, 37–42 (2018).

7. Shinoda, K. & Fujitani, H. Initiation of prolyl cis-trans isomerisation in the CDR-H3 loop of an antibody in response to antigen binding. *Sci. Rep.* **7**, 16964 (2017).

8. Joseph, A. P., Srinivasan, N. & de Brevern, A. G. Cis-trans peptide variations in structurally similar proteins. *Amino Acids* **43**, 1369–1381 (2012).

9. Wernisch, S., Trapp, O. & Lindner, W. Application of cinchona-sulfonate-based chiral zwitterionic ion exchangers for the separation of proline-containing dipeptide rotamers and determination of on-column isomerization parameters from dynamic elution profiles. *Anal. Chim. Acta* **795**, 88–98 (2013).

10. Yao, J. *et al.* Stabilization of a type VI turn in a family of linear peptides in water solution. *J. Mol. Biol.* **243**, 736–753 (1994).

11. Schmidpeter, P. A. M., Koch, J. R. & Schmid, F. X. Control of protein function by prolyl isomerization. *Biochim. Biophys. Acta BBA - Gen. Subj.* **1850**, 1973–1982 (2015).

12. Vogel, M., Bukau, B. & Mayer, M. P. Allosteric regulation of Hsp70 chaperones by a proline switch. *Mol. Cell* **21**, 359–367 (2006).

13. Nicholson, L. K. & Lu, K. P. Prolyl cis-trans Isomerization as a Molecular Timer in Crk Signaling. *Mol. Cell* **25**, 483–485 (2007).

14. Nath, P. R. & Isakov, N. Insights into peptidyl-prolyl cis–trans isomerase structure and function in immunocytes. *Immunol. Lett.* **163**, 120–131 (2015).

15. Sarkar, P., Reichman, C., Saleh, T., Birge, R. B. & Kalodimos, C. G. Proline cis-trans Isomerization Controls Autoinhibition of a Signaling Protein. *Mol. Cell* **25**, 413–426 (2007).

16. Xia, J. & Levy, R. M. Molecular Dynamics of the Proline Switch and Its Role in Crk Signaling. *J. Phys. Chem. B* **118**, 4535–4545 (2014).

17. Wulf, G., Finn, G., Suizu, F. & Lu, K. P. Phosphorylation-specific prolyl isomerization: is there an underlying theme? *Nat. Cell Biol.* **7**, 435–441 (2005).

18. Zhou, X. Z., Lu, P. J., Wulf, G. & Lu, K. P. Phosphorylation-dependent prolyl isomerization: a novel signaling regulatory mechanism. *Cell. Mol. Life Sci. CMLS* **56**, 788–806 (1999).

19. Takahashi, K., Uchida, C., Shin, R.-W., Shimazaki, K. & Uchida, T. Prolyl isomerase, Pin1: new findings of post-translational modifications and physiological substrates in cancer, asthma and Alzheimer's disease. *Cell. Mol. Life Sci. CMLS* **65**, 359–375 (2008).

20. Chen, S.-Y. *et al.* Activation of beta-catenin signaling in prostate cancer by peptidyl-prolyl isomerase Pin1-mediated abrogation of the androgen receptor-beta-catenin interaction. *Mol. Cell. Biol.* **26**, 929–939 (2006).

21. Cao, W. *et al.* BCR-ABL enhances the prolyl isomerase activity of Pin 1 by interacting with DAPK1 in ph+ ALL. *Cancer Med.* **7**, 2530–2540 (2018).

22. Chen, Y. *et al.* Prolyl isomerase Pin1: a promoter of cancer and a target for therapy. *Cell Death Dis.* **9**, 883 (2018).

23. Pastorino, L. *et al.* The prolyl isomerase Pin1 regulates amyloid precursor protein processing and amyloid-beta production. *Nature* **440**, 528–534 (2006).

24. Feige, M. J., Walter, S. & Buchner, J. Folding mechanism of the CH2 antibody domain. *J. Mol. Biol.* **344**, 107–118 (2004).

25. Thies, M. J. *et al.* Folding and association of the antibody domain CH3: prolyl isomerization preceeds dimerization. *J. Mol. Biol.* **293**, 67–79 (1999).

26. Jäger, M. & Plückthun, A. The rate-limiting steps for the folding of an antibody scFv fragment. *FEBS Lett.* **418**, 106–110 (1997).

27. Lilie, H., Lang, K., Rudolph, R. & Buchner, J. Prolyl isomerases catalyze antibody folding in vitro. *Protein Sci. Publ. Protein Soc.* **2**, 1490–1496 (1993).

28. Wu, X. *et al.* Rational Design of Envelope Identifies Broadly Neutralizing Human Monoclonal Antibodies to HIV-1. *Science* **329**, 856–861 (2010).

29. Pegu, A. *et al.* Neutralizing antibodies to HIV-1 envelope protect more effectively in vivo than those to the CD4 receptor. *Sci. Transl. Med.* **6**, 243ra88 (2014).

30. Sok, D. *et al.* Recombinant HIV envelope trimer selects for quaternary-dependent antibodies targeting the trimer apex. *Proc. Natl. Acad. Sci. U. S. A.* **111**, 17624–17629 (2014).

31. Kwon, Y. D. *et al.* Optimization of the Solubility of HIV-1-Neutralizing Antibody 10E8 through Somatic Variation and Structure-Based Design. *J. Virol.* **90**, 5899–5914 (2016).

32. Steinmetz, A. *et al.* CODV-Ig, a universal bispecific tetravalent and multifunctional immunoglobulin format for medical applications. *mAbs* **8**, 867–878 (2016).

33. Hawe, A., Sutter, M. & Jiskoot, W. Extrinsic Fluorescent Dyes as Tools for Protein Characterization. *Pharm. Res.* **25**, 1487–1499 (2008).

34. Hamelberg, D., Mongan, J. & McCammon, J. A. Accelerated molecular dynamics: a promising and efficient simulation method for biomolecules. *J. Chem. Phys.* **120**, 11919–11929 (2004).

35. Chen, Y. *et al.* Prolyl isomerase Pin1: a promoter of cancer and a target for therapy. *Cell Death Dis.* **9**, 883 (2018).

36. Takahashi, K., Uchida, C., Shin, R.-W., Shimazaki, K. & Uchida, T. Prolyl isomerase, Pin1: new findings of post-translational modifications and physiological substrates in cancer, asthma and Alzheimer's disease. *Cell. Mol. Life Sci.* **65**, 359–375 (2008).

37. Feige, M. J., Hendershot, L. M. & Buchner, J. How antibodies fold. *Trends Biochem. Sci.* **35**, 189–198 (2010).

38. Feige, M. J. & Buchner, J. Principles and engineering of antibody folding and assembly. *Biochim. Biophys. Acta* **1844**, 2024–2031 (2014).

39. Georgiev, I. S. *et al.* Antibodies VRC01 and 10E8 neutralize HIV-1 with high breadth and potency even with Ig-framework regions substantially reverted to germline. *J. Immunol. Baltim. Md 1950* **192**, 1100–1106 (2014).

40. Chennamsetty, N., Voynov, V., Kayser, V., Helk, B. & Trout, B. L. Prediction of Aggregation Prone Regions of Therapeutic Proteins. (2010). doi:10.1021/jp911706q

41. Phillips, J. C. *et al.* Scalable molecular dynamics with NAMD. *J. Comput. Chem.* **26**, 1781–1802 (2005).

42. MacKerell, A. D., Banavali, N. & Foloppe, N. Development and current status of the CHARMM force field for nucleic acids. *Biopolymers* **56**, 257–265 (2000).

43. Glykos, N. M. Software news and updates. Carma: a molecular dynamics analysis program. *J. Comput. Chem.* **27**, 1765–1768 (2006).

44. Skjærven, L., Yao, X.-Q., Scarabelli, G. & Grant, B. J. Integrating protein structural dynamics and evolutionary analysis with Bio3D. *BMC Bioinformatics* **15**, 399 (2014).

45. Humphrey, W., Dalke, A. & Schulten, K. VMD: visual molecular dynamics. *J. Mol. Graph.* **14**, 33–38, 27–28 (1996).

Tables

Table 1. Kinetic analysis of the Conformers I and II and the unseparated conformers by ForteBio Octet 96.

	Conformer I	**Conformer II**	**Unseparated conformers (equilibrium)**
KD (nM)	2.96E-07	2.8E-08	3.0E-08
ka (/1Ms)	4.5E+03	4.68E+04	2.90E+04
kd (1/s)	1.26E-03	1.28E-03	8.78E-04

Figure legends

Figure 1. (**A**) UHPLC-SEC of SAR441236 showing the two peaks profile. (**B**) Apparent mass and hydrodynamic radius (Rh) by SEC-LS of SAR441236. Both peaks show the same apparent molecular weight in SEC-LS = ~ 200kDa and a Rh = ~ 6.4nm. (**C**) Deconvoluted MS spectrum of deglycosylated SAR441236 in denaturing conditions. (**D**) SEC profile of each fraction (Fraction 1-black, Fraction 2-blue) 30-60 min after collections (left) and after 72h (right) at 8°C in Dulbecco phosphate-buffered saline (DPBS2X). (**E**) Kinetics of conformer ratio after 5 times dilution in pH 5.0 buffer and 5 times dilution in pH 7.0 buffer. Conformer I "open" is depicted in blue empty squares, conformer II "closed" is depicted in red empty circles.

Figure 2. (**A**) enzymatic cleavage, (**B**) Total Ion Current (TIC), (**C**)-(**E**) deconvoluted spectra of the three major peaks. The peak of each conformer (conformation I – blue and conformation II – red) found in the CODV arm show the same Mass. (**B**)-(**E**) The blue arrow on the y-axis is an annotation threshold given by the software representing the lowest threshold to show peaks annotation.

Figure 3. Structural superposition between 10e8v4 CODV and Fab crystal structures. (**A**) Highlighted difference (red circle) between 10e8v4 HCDR3 of CODV (purple) – "open" conformation (conformation I) and Fab (blue) – "closed" conformation (conformation II). (**B**) The trans dihedral angle of the CODV P113 (cyan) and the cis dihedral angle of Fab P113 (yellow). (**C**) Topology of H147 with respect to YPP motif (Heavy Chain - Red) and R207 (Light Chain – Blue).

Figure 4. ELISA optical density (OD) at different concentrations for (**A**) reference batch vs conformer I "open", (**B**) reference batch vs conformer II "closed" and (**C**) conformer I "open" vs conformer II "closed"

Figure 5. Plot of the kinetic of the three peaks (Conformer I "open" – blue / Conformer II "closed" – red /complex mAb-Ag – green) followed by LC/MS, based on the peak area surface.

Figure 6. (**A**) Heat map of the preferred P112-P113 conformations obtained by 4x100 ns accelerated molecular dynamics. The most populated transition state is highlighted within orange dotted box. A dihedral value of 0° corresponds to the *cis* conformers, values close to

180° or -180° correspond to *trans* conformers. (**B**) Histogram plot of the dihedral angle of P112 (red) and P113 (green) vs the relative dihedral population density.

Figure 7. (**A**) Native SEC analysis UV trace of the mutants versus the reference material and (**B**) ELISA binding curves of the reference batch (black), Var1 (blue), Var2 (red), Var3 (green), Var4 (purple) and Var5 (cyan).

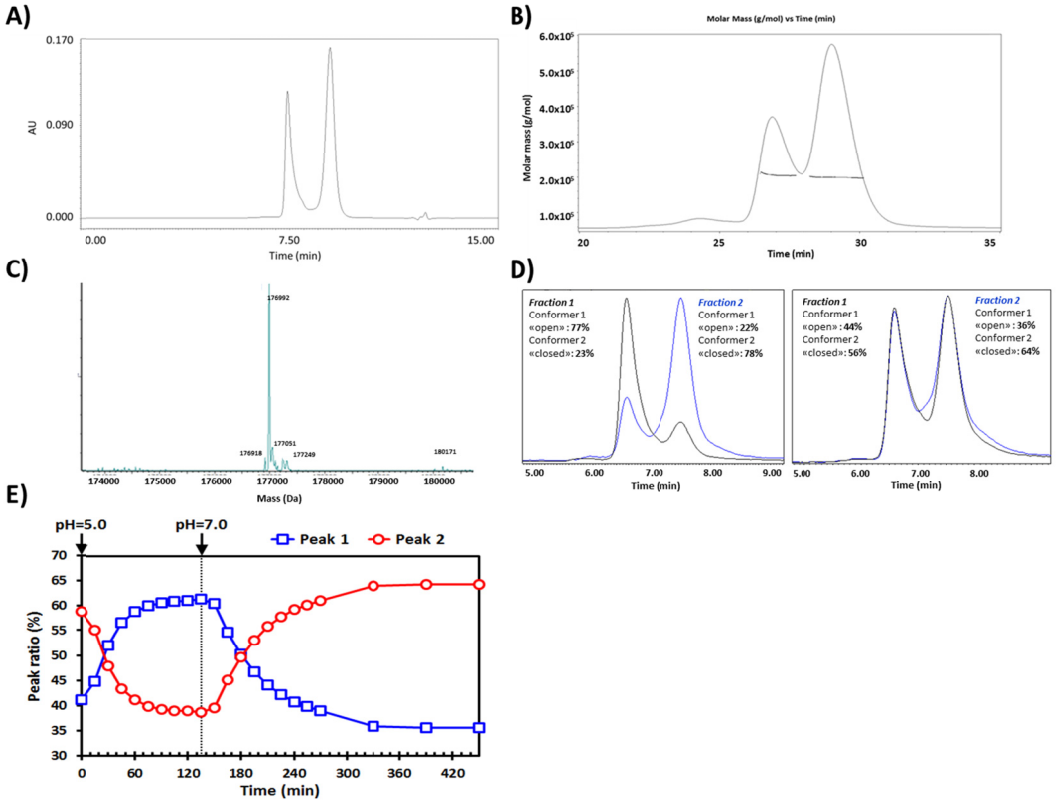

Figure 1: A) UHPLC-SEC of SAR441236 showing the two peaks profile. B) Apparent mass and hydrodynamic radius (Rh) by SEC-LS of SAR441236. Both peaks show the same apparent molecular weight in SEC-LS = ~ 200kDa and a Rh = ~ 6.4nm. C) Deconvoluted MS spectrum of deglycosylated SAR441236 in denaturing conditions. D) SEC profile of each fraction (Fraction 1-black, Fraction 2-blue) 30-60 min after collections (left) and after 72h (right) at 8°C in Dulbecco Phosphate-Buffered Saline (DPBS2X). E) Kinetics of conformer ratio after 5 times dilution in pH 5.0 buffer and 5 times dilution in pH 7.0 buffer. Conformer I "open" is depicted in blue empty squares, conformer II "closed" is depicted in red empty circles.

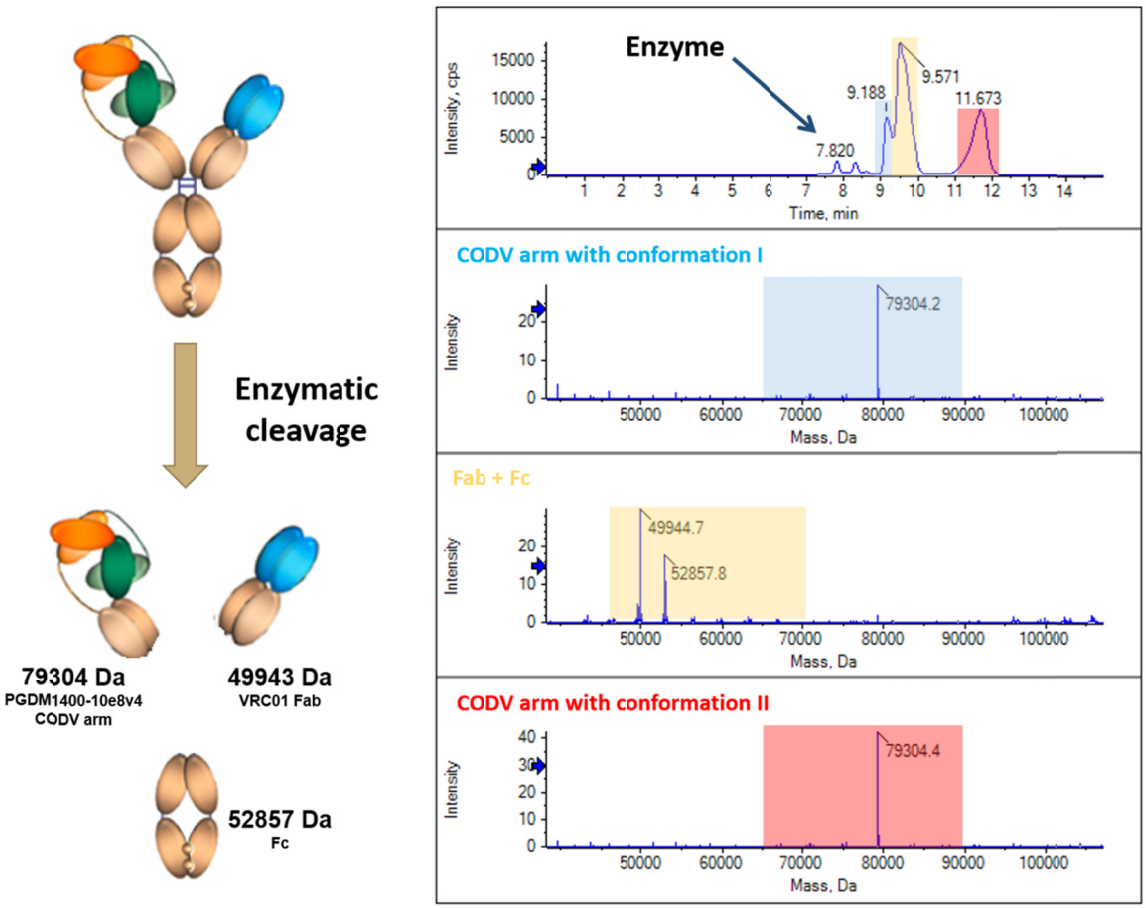

Figure 2: Native SEC-UV/MS on subunits of SAR441236– deconvoluted spectra of the three major peaks. The peak of each conformer (conformation I – blue and conformation II – red) found in the CODV arm show the same Mass.

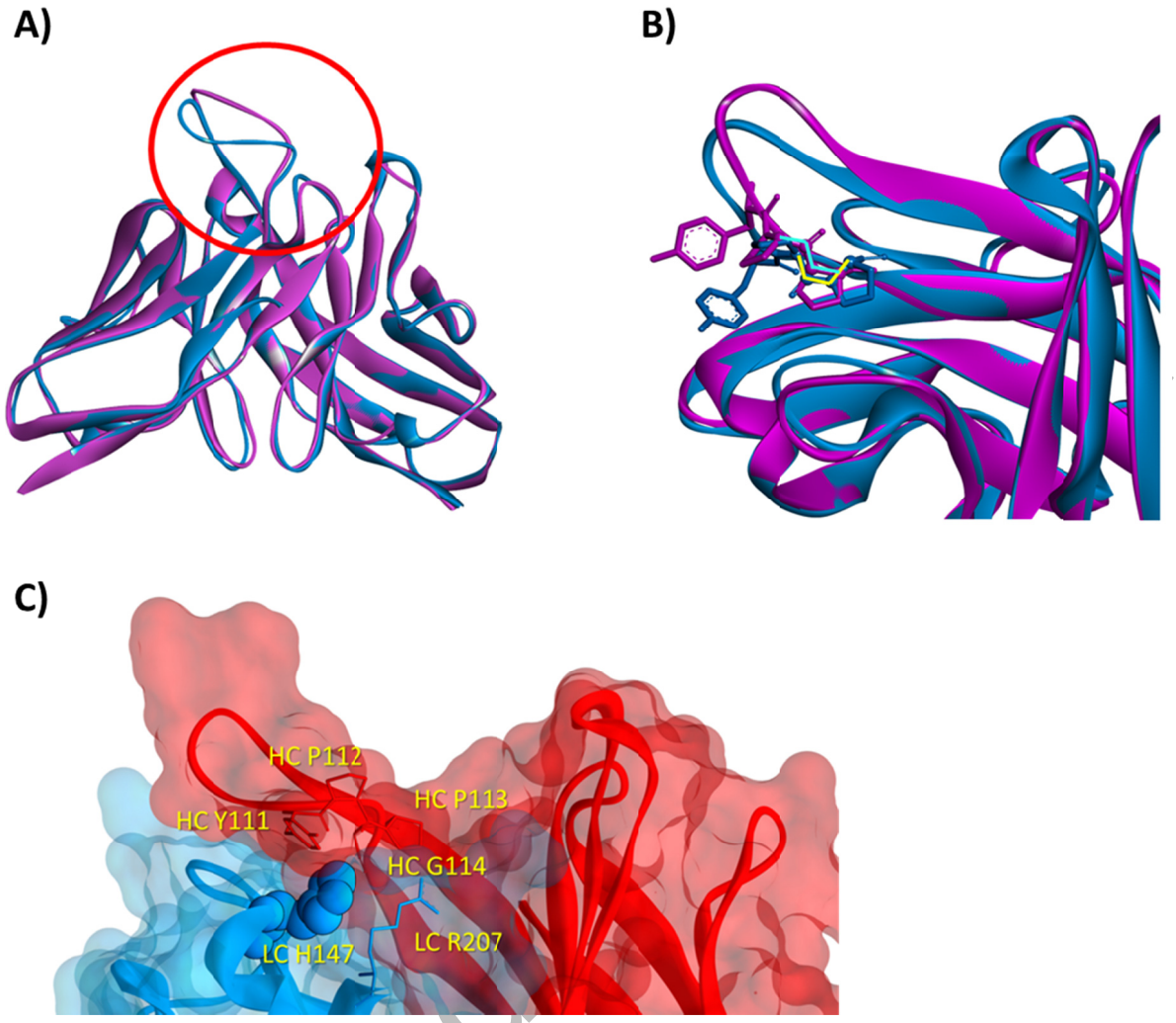

Figure 3: Structural superposition between 10e8v4 CODV and Fab crystal structures. A) Highlighted difference (red circle) between 10e8v4 HCDR3 of CODV (purple) and Fab (blue). B) The *trans* dihedral angle of the CODV P113 (cyan) and the *cis* dihedral angle of Fab P113 (yellow). C) Topology of H147 with respect to YPP motif (Heavy Chain - Red) and R207 (Light Chain – Blue).

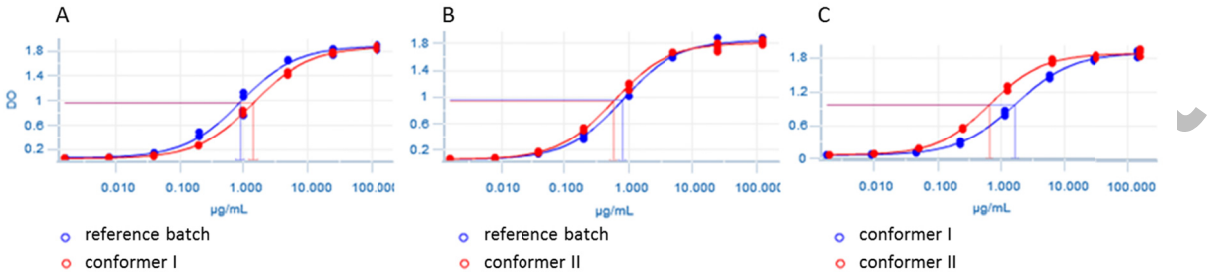

Figure 4: ELISA optical density (OD) at different concentrations for A) reference batch vs Conformer I, B) reference batch vs conformer II and C) conformer I "open" vs conformer II "closed"

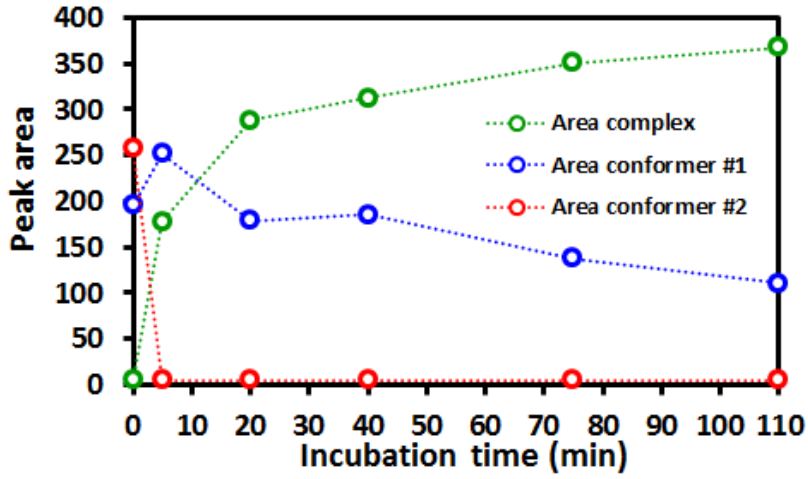

Figure 5: Plot of the kinetic of the three peaks (Conformer I "open" – blue / Conformer II "closed" – red /complex mAb-Ag – green) followed by LC/MS, based on the peak area surface

A)

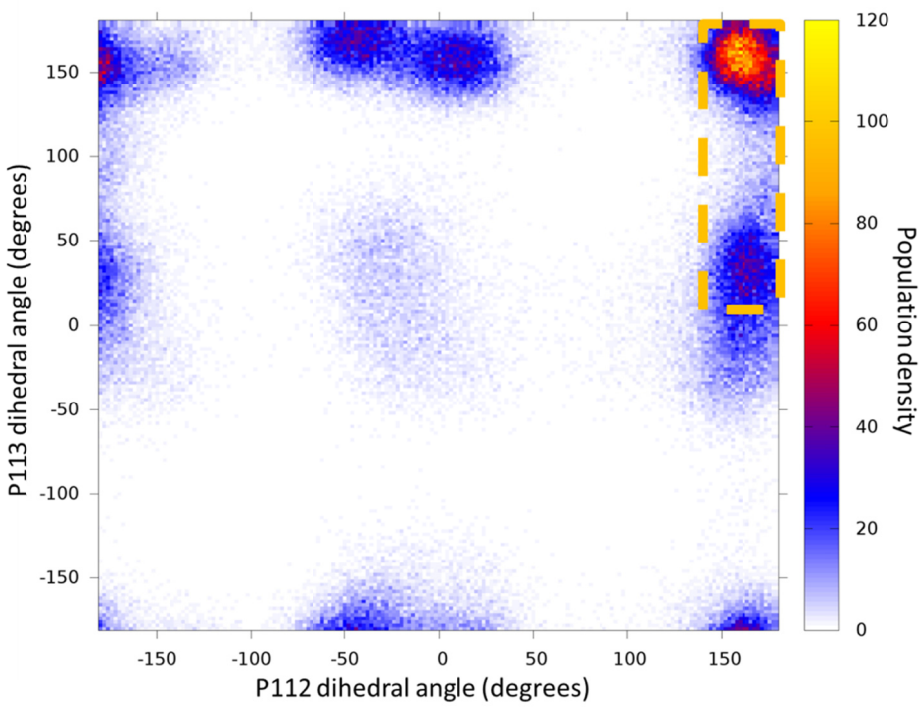
P113 dihedral angle (degrees)
150
100
50
0
-50
-100
-150
-150
-100
-50
0
50
100
150
P112 dihedral angle (degrees)
120
100
80
60
40
20
0
Population density

B)

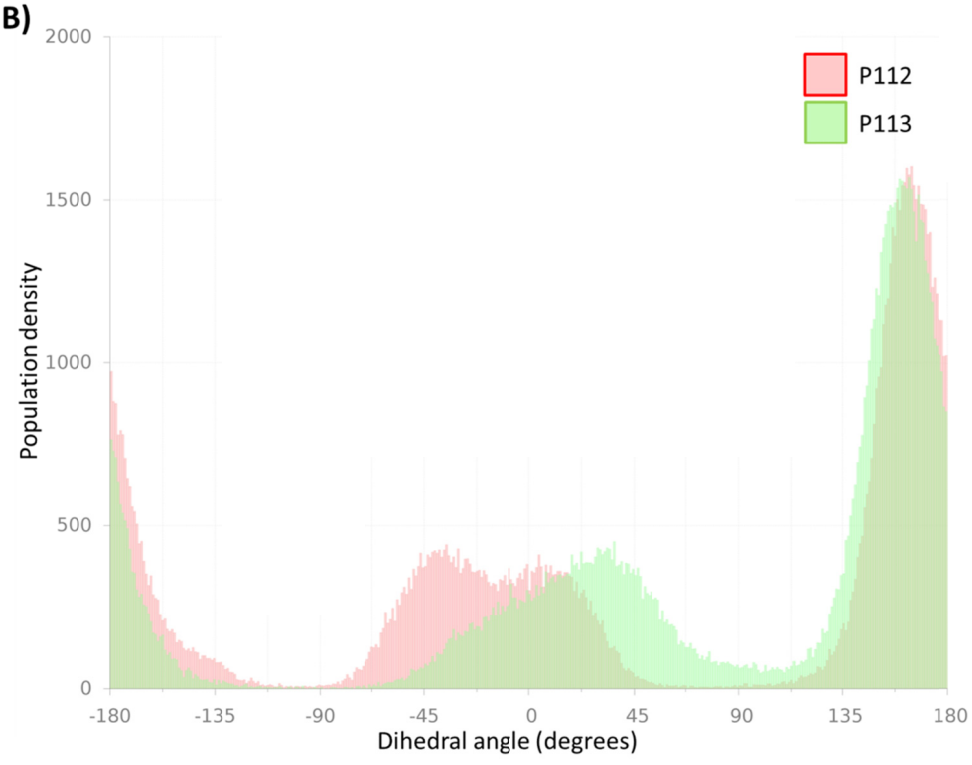
2000
1500
1000
500
0
Population density
P112
P113
-180
-135
-90
-45
0
45
90
135
180
Dihedral angle (degrees)

Figure 6: A) Heat map of the preferred P112-P113 conformations obtained by 4x100ns accelerated molecular dynamics. The most populated transition state is highlighted within orange dotted box. A dihedral value of 0^0 corresponds to the *cis* conformer, values close to 180^0 or -180^0 correspond to *trans* conformers. B) Histogram plot of the dihedral angle of P112 (red) and P113 (green) vs the relative dihedral population density.

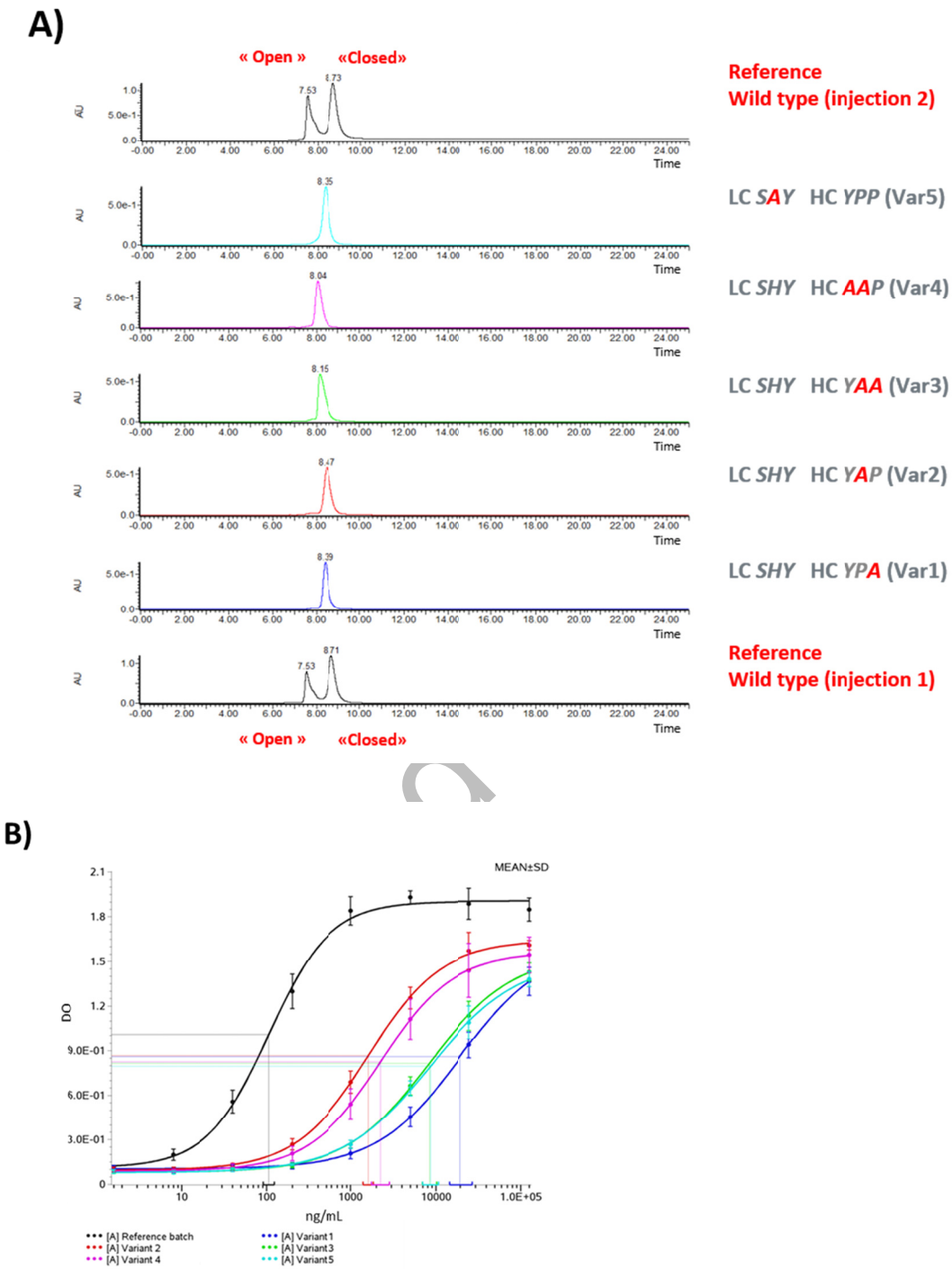

Figure 7: A) Native SEC analysis UV trace of the mutants versus the reference material and B) ELISA binding curves of the reference batch (black), Var1 (blue), Var2 (red), Var3 (green), Var4 (purple) and Var5 (cyan).